CANCER

Programmable probiotics for detection of cancer in urine

Tal Danino,[1]* Arthur Prindle,[2]* Gabriel A. Kwong,[1†] Matthew Skalak,[1] Howard Li,[2] Kaitlin Allen,[1] Jeff Hasty,[2,3,4‡] Sangeeta N. Bhatia[1,5,6,7,8‡§]

Rapid advances in the forward engineering of genetic circuitry in living cells has positioned synthetic biology as a potential means to solve numerous biomedical problems, including disease diagnosis and therapy. One challenge in exploiting synthetic biology for translational applications is to engineer microbes that are well tolerated by patients and seamlessly integrate with existing clinical methods. We use the safe and widely used probiotic *Escherichia coli* Nissle 1917 to develop an orally administered diagnostic that can noninvasively indicate the presence of liver metastasis by producing easily detectable signals in urine. Our microbial diagnostic generated a high-contrast urine signal through selective expansion in liver metastases (10^6-fold enrichment) and high expression of a lacZ reporter maintained by engineering a stable plasmid system. The lacZ reporter cleaves a substrate to produce a small molecule that can be detected in urine. *E. coli* Nissle 1917 robustly colonized tumor tissue in rodent models of liver metastasis after oral delivery but did not colonize healthy organs or fibrotic liver tissue. We saw no deleterious health effects on the mice for more than 12 months after oral delivery. Our results demonstrate that probiotics can be programmed to safely and selectively deliver synthetic gene circuits to diseased tissue microenvironments in vivo.

INTRODUCTION

The pervasive beneficial microbial species in and on the human body are important for the maintenance of mammalian homeostasis, as revealed by studies on the human microbiome (*1*, *2*). Even more remarkable, microbes are present in diverse organs and tissues previously thought to be sterile environments, including tumors (*3*, *4*). Empirical studies dating back to the 19th century suggested that bacteria can affect tumor growth (*5*), and recent work has demonstrated that microbes directly administered intravenously can grow selectively in tumors without adversely affecting the health of the host (*6*–*8*). This phenomenon has been attributed to suppressed immune surveillance within the tumor and increased availability of nutrients in the necrotic tumor core, prompting the exploration of tumor-specific bacterial growth as a mode of cancer therapy and diagnosis (*6*–*14*). Specifically, the ability of bacteria to selectively home to tumors raises the possibility of using microbes as programmable delivery vehicles for therapeutic or diagnostic agents. Although such microbial approaches have, to date, been primarily limited to obligate anaerobes, common laboratory strains readily amenable to genetic engineering such as *Salmonella typhimurium* and *Escherichia coli* also home to tumors (*6*, *15*, *16*), potentially allowing the incorporation of specialized genetic circuitry to fight cancer.

Synthetic biology is an interdisciplinary engineering process in which computational modeling and experimental manipulation produce specified, genetically controlled behavior in bacteria. This forward engineering approach can generate a variety of genetic programs including switches, oscillators, counters, edge detectors, and biosensors (*17*–*23*). These successes have stimulated interest in reprogramming bacteria for biomedical applications, with early examples including engineered phage for biofilm dispersal (*24*), and commensal bacteria designed to combat diabetes (*25*), HIV (*26*), and cholera (*27*) by producing small molecules directly in the gastrointestinal tract.

Bacteria have a natural propensity to colonize tumor environments, and although bacteria have been administered safely in human clinical trials for cancer treatment, efficient tumor colonization requires administration of high concentrations of bacteria directly into the bloodstream (*9*, *28*, *29*) and therefore has a narrow therapeutic index. We sought to improve tolerability of this approach by developing a method to deliver bacteria to tumors that would use lower concentrations of circulating bacteria. Here, we have therefore explored oral administration of nonvirulent probiotic strains as a path to selectively colonize tumors while minimizing systemic exposure. We reasoned that oral delivery could lead to the preferential colonization of liver tumors by allowing probiotics to follow physiological blood flow patterns, wherein the venous outflow from the gut is directed to the liver via the hepatic portal vein. We also reasoned that the liver may be an ideal organ to target with oral delivery, because it is the primary site of metastasis for several tumor types including colorectal, breast, and pancreatic (*30*, *31*).

The metastatic spread of cancer is ultimately responsible for 90% of all cancer-related deaths, and liver metastases represent an enormous clinical challenge, in large part because of their small size and multiplicity (*30*). However, compared to other sites of metastasis (for example, bone and brain), treatment options that leverage the remarkable regenerative capacity of the liver are advancing. Local resection, radiation, and radio frequency ablation are all being explored as therapeutic approaches to focal liver metastases (*32*, *33*). To date, patients with liver-confined colorectal metastases that undergo local therapy have 5-year survival rates of ~30 to 50% (*34*). However, only ~6% of patients ultimately undergo a curative resection (*35*), likely because of the relatively

[1]Institute for Medical Engineering and Science, Massachusetts Institute of Technology (MIT), Cambridge, MA 02139, USA. [2]Department of Bioengineering, University of California, San Diego, La Jolla, CA 92093, USA. [3]BioCircuits Institute, University of California, San Diego, La Jolla, CA 92093, USA. [4]Molecular Biology Section, Division of Biological Science, University of California, San Diego, La Jolla, CA 92093, USA. [5]Broad Institute of Harvard and MIT, Cambridge, MA 02142, USA. [6]Department of Medicine, Brigham and Women's Hospital, Boston, MA 02115, USA. [7]Electrical Engineering and Computer Science and David H. Koch Institute for Integrative Cancer Research, MIT, Cambridge, MA 02139, USA. [8]Howard Hughes Medical Institute, Chevy Chase, MD 20815, USA.
*Equally contributing lead authors.
†Present address: Wallace H. Coulter Department of Biomedical Engineering, Georgia Tech and Emory School of Medicine, Atlanta, GA 30332, USA.
‡Equally contributing senior authors.
§Corresponding author. E-mail: sbhatia@mit.edu

late stage of the initial detection of the metastases. Thus, the need for methods in addition to standard imaging modalities that can detect liver metastases while preserving curative treatment options is of paramount importance. Here, we sought to develop a simple method for oral delivery of the probiotic bacterium *E. coli* Nissle 1917 (EcN), engineered to carry specific gene circuits that enable tumor detection in urine, to liver metastases.

RESULTS

Designing programmable probiotics for diagnostic applications

Motivated by the need for an accessible, highly sensitive, and selective tool for detection of small metastases that are beyond the reach of existing diagnostic tools, we engineered a bacterial strain, EcN, with a series of expression cassettes. The predominant EcN platform used in this study, PROP-Z (programmable probiotics with lacZ; Table 1), harbors both (i) a genomically integrated erythromycin-resistant luxCDABE cassette (*36*) to generate a luminescent signal from endogenous production of bacterial luciferin and luciferase (*36*, *37*) and (ii) a pTKW106alp7A plasmid (fig. S1, constructed for this study) that provides kanamycin resistance, isopropyl-β-D-thiogalactopyranoside (IPTG)–inducible lacZ expression, and an engineered plasmid maintenance system (see below). This PROP-Z construct produces two important functional outputs. First, PROP-Z bacteria produce a luminescent signal that is detectable both in vitro and by whole-animal imaging. Furthermore, this signal can be discriminated from luminescence generated by luciferase produced in engineered mammalian cells (see Materials and Methods). Second, diverse products of lacZ enzymatic activity can serve as colorimetric, fluorescent, or luminescent readouts to indicate activity-based cleavage of engineered substrates. The output of PROP-Z can be controlled by providing various luciferase and lacZ substrates, and subspecies of PROP-Z bacteria can be engineered to regulate the expression or activity of either enzyme (Table 1). For example, PROP-Z will

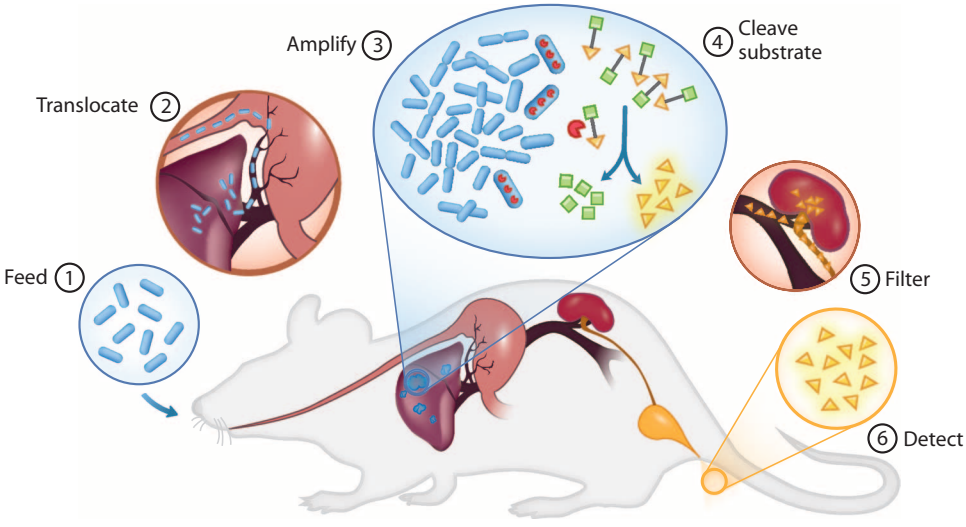

Fig. 1. PROP-Z probiotics for noninvasive cancer detection. The PROP-Z diagnostic platform is made up of probiotic EcN bacteria transformed with a dual-stabilized, high-expression lacZ vector as well as a genomically integrated luxCDABE cassette that allows for luminescent visualization without providing exogenous luciferin (blue). (1) PROP-Z is delivered orally. (2) Probiotics rapidly (within 24 hours) translocate across the gastrointestinal tract and (3) specifically amplify within metastatic tumors present in the liver. (4) PROP-Z expresses high levels of the enzyme lacZ (red), which can cleave systemically injected, cleavable substrates (green and yellow). Cleavage products of the substrates (yellow) filter through the renal system (5) into the urine for detection (6).

Table 1. Bacterial strains and mammalian cell types used in this study. AHL, *N*-(3-oxohexanoyl)-L-homoserine lactone; GEMM, genetically engineered mouse model.

Label	Bacterial strain or mammalian cell	Genomic/plasmids	Use(s)
PROP-Z	EcN	luxCDABE (genomic), IPTG-inducible lacZ (stabilized plasmid)	Bioluminescent imaging of bacteria, urine diagnostic assay
PROP-Luc	EcN	luxCDABE (genomic), luxCDABE (plasmid)	Bioluminescent imaging of bacteria
PROPi-Luc	EcN	AHL-inducible luxCDABE (plasmid)	Bioluminescent imaging of bacteria
Non-lacZ	Mach One	lacZΔM15 (genomic mutant)	Non-lacZ control for urine diagnostic assay
MC26-LucF	Metastatic colorectal mouse cell line	Firefly luciferase (genomic)	Subcutaneous xenografts and liver metastasis models
LS174T-LucF	Human colorectal adenocarcinoma cell line	Firefly luciferase (genomic)	Subcutaneous xenograft models
393M1-LucF	GEMM lung mouse cell line	Firefly luciferase (genomic)	Subcutaneous xenografts and liver metastasis models

only produce lacZ when exposed to the inducing agent IPTG. Specifically, we sought to develop a versatile PROP-Z platform to act as a synthetic diagnostic tool for the detection of liver metastasis via the urine (Fig. 1).

PROP delivered orally colonizes experimental liver metastases

To determine the efficiency with which PROP bacteria, delivered orally, can colonize liver metastases, we established a murine model of colorectal cancer metastases in the liver by surgically injecting a metastatic murine colorectal cell line (MC26-LucF) (Table 1) into the spleen of immunocompetent Balb/c host mice (Fig. 2A). We visualized the growth of individual liver metastases by magnetic resonance imaging (MRI) in the same mouse at two time points (14 and 17 days after injection) and quantified the distribution of tumor sizes at the 14-day time point in 10 mice, where the average tumor diameters were about 1.5 mm (Fig. 2, B and C). The growth of metastases was additionally monitored between 1 to 3 weeks by IVIS (in vivo imaging system) after intraperitoneal injection of D-luciferin, the substrate for the firefly luciferase expressed by the tumor cell line (Fig. 2, D and E). When luminescent signals reached 1×10^9 to 5×10^9 radiance (photons $s^{-1}cm^{-2}$ sr^{-1}), corresponding to average tumor diameters of ~2 to 3 mm, we orally administered PROP-Luc (Table 1) and observed strong bacterial-derived luminescent signals in most metastases in excised livers, including in tumors as small as 1 mm (Fig. 3A). In addition, we did not see bacterial-derived luminescent signals arising from nontumor tissue. We quantified the efficiency of PROP-Luc colonization and found that 88% of 83 tumor metastases, ranging from 1 to 8 mm in diameter, exhibited a bacteria-derived luminescent signal (Fig. 3B, fig. S2, and table S1). This method confirmed the presence of liver metastases and allowed their visualization in the entire liver by a noninvasive approach. Together, these results demonstrate that orally administered probiotics have the capacity to cross the gastrointestinal tract and colonize large and small hepatic metastases.

Oral probiotics specifically colonize multiple models of cancer and liver metastases

To test the liver specificity of colonization, we developed a quantitative PCR (qPCR)–based assay (fig. S3) and measured the number of orally administered PROP-Z bacteria that colonized host organs, including the spleen, the other major organ with known reticuloendothelial filtration function (*38*). At 24 hours after oral administration of PROP-Z, liver metastases contained a striking level of colonization: $5 \times 10^6 \pm 1 \times 10^6$ bacteria per gram of liver tissue ($n = 3$ livers; Fig. 3C). In contrast, PROP-Z levels in healthy spleen, kidneys, and liver were below the limits of detection of our qPCR assay (<500 bacteria per gram of tissue), even after 7 days past PROP-Z administration to allow for bacterial growth. We also performed colony counts of entire organs in case the colonization was lower than the 500 bacteria per gram detection limit, but even then could not detect evidence of PROP-Z bacteria in any control organ tested (Fig. 3C). This absence of colonization by orally delivered PROP-Z was further corroborated by histological analysis of tissue sections (brain, spleen, liver, kidney, heart, and lung), which revealed no indication of inflammation, tissue damage, or cell death (fig. S4). PROP-Z–treated mice survived with no apparent adverse effects for at least 12 months. These findings demonstrate

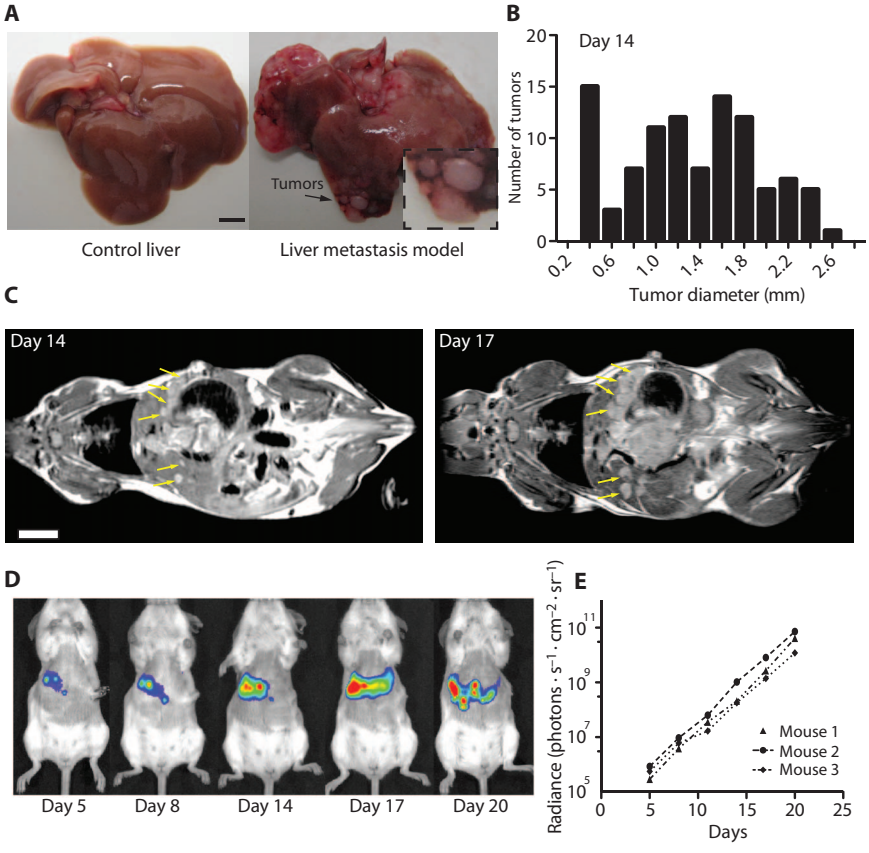

Fig. 2. Colonization of liver metastases by orally administered probiotics. (**A**) Representative healthy and tumor-bearing livers from Balb/c mice, excised ~21 days after intrasplenic injection of MC26-LucF cells bearing a firefly luciferase transgene. Arrow, small tumor nodules typical of those arising in this metastasis model. Scale bar, 5 mm. (**B**) Frequency distribution of tumor diameters in mice carrying MC26-LucF liver metastases 14 days after injection of the cells as measured by MRI. $n = 10$ mice, 98 tumors. (**C**) MRI images of a mouse with MC26-LucF liver metastases 14 and 17 days after injection of MC26-LucF cells. Yellow arrows, metastases. Scale bar, 10 mm. (**D**) Representative IVIS images for luminescence of MC26-LucF:Balb/c liver metastasis mice monitored over 21 days. (**E**) Average radiance for three mice shown as a function of time.

that oral delivery of the probiotic EcN is well tolerated by the host and leads to specific colonization of hepatic tumors by EcN without triggering systemic responses.

Next, we sought to investigate the specificity with which PROP can colonize tumor microenvironments relative to other liver injury settings. Because liver fibrosis is a final end result to a diverse array of liver insults, we induced liver fibrosis in mice by allowing them to freely ingest rodent chow containing the hepatotoxin DDC (3,5-diethoxycarbonyl-1,4-dihydrocollidine) (*39*). After 3 weeks, we verified the induction of liver fibrosis in tissue sections (Fig. 3D) and, in a parallel cohort of mice, found that orally delivered PROP-Z did not colonize fibrotic tissue, as measured by colony counts (Fig. 3E). Together, these data indicate that oral delivery of PROP-Z achieves robust and specific colonization of metastases while, unlike intravenous delivery, yielding minimal concentrations of bacteria in blood and off-target organs.

To explore the dose dependence and potential for colonization by PROP in tumors with different origins, we established subcutaneous tumors derived from human ovarian (TOV21G) and colorectal (LS174T-LucF) tumors, as well as murine colon (MC26-LucF), lung (393M1-LucF), and pancreatic (KBP22) tumors, the latter two derived from GEMM (*40*). To ensure that these subcutaneous tumors were exposed to similar levels of probiotic, we delivered a single high dose of PROP-Z (5×10^6 CFU) by systemic intravenous injection and observed complete colonization of subcutaneous tumors in all but the lung tumor model (83% colonized) (Fig. 4, A and B). To assay whether the tumors from varying genetic backgrounds exhibit different thresholds for colonization, we compared the dosage requirements for colonization after both oral administration and traditional intravenous delivery in two models. We administered PROP-Z intravenously to mice bearing subcutaneous tumors with bacterial levels ranging from 10^4 to 5×10^6 CFU and observed a dose-dependent increase in the frequency of tumor colonization in both immunocompetent and compromised hosts (Fig. 4, C and D). In marked contrast to intravenous delivery, we found that oral delivery of PROP-Z (5×10^9 CFU) at doses well above our intravenous concentrations failed to colonize subcutaneous tumors (Fig. 4, C and D), but the same doses led to colonization of liver metastases derived from two metastatic cell lines (393M1-LucF and MC26-LucF). Given the ability of intravenously administered bacteria to colonize a range of tumor types both in animal models and in a spectrum of clinical settings (*7*–*13*, *41*), we reasoned that propensity for tumor colonization may depend more on the local concentration of bacteria than on the tumor type per se.

These results suggested that oral delivery results in a markedly lower circulating level of bacteria than intravenous delivery. To test this hypothesis, we counted the number of bacteria in the blood at time points between 1 and 24 hours after oral delivery of PROP-Z and found no evidence of circulating bacteria above our detection limit of 10^3 CFU/ml of blood. The observation that both liver metastasis models and five subcutaneous cancer models were susceptible to colonization is consistent with the conclusion that PROP will selectively colonize tumors over healthy organs in a dose-dependent manner. Collectively, these findings demonstrated colonization of diverse liver metastases by oral delivery of the probiotic EcN, suggesting that this programmable probiotic may be an appropriate vehicle for developing an oral, broad-spectrum diagnostic for cancers that frequently result in liver metastases.

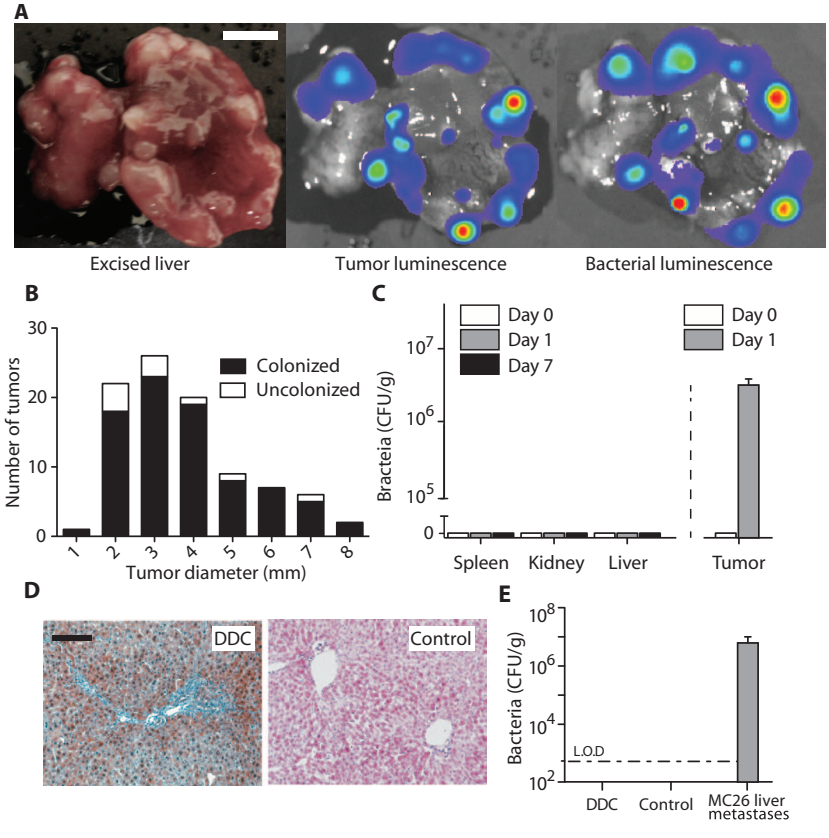

Fig. 3. Colonization of liver metastases by orally delivered PROP: Quantitation and specificity. (**A**) Twenty-four hours after oral delivery of PROP-Luc [5×10^9 colony-forming units (CFU)] to Balb/c mice carrying liver metastases (at 21 days), livers were excised and photographed (left), imaged for bacterial luminescence with IVIS (right), and then soaked in luciferin to visualize tumors with active mammalian MC26-LucF–derived luminescence (middle). Scale bars, 10 mm. (**B**) Distribution of colonized and uncolonized liver metastases from three mouse livers. Tumor diameters and colonization were determined by overlaying IVIS images, as described in Materials and Methods and fig. S2. (**C**) PROP-Z present in organs of healthy Balb/c mice (left) or liver metastases–bearing mice (right) after oral administration were quantified by traditional colony counting on erythromycin-LB plates and confirmed by a qPCR-based assay. Data represent mean colony counts from organs from $n = 4$ mice ± SEM. (**D**) Mice bearing DDC-induced liver injury (fibrotic damage visualized by a hematoxylin and eosin stain) were gavaged with 5×10^9 CFU PROP-Z. Excised livers were examined by IVIS. (**E**) Bacteria levels in liver metastases of control, DDC-treated animals, or Balb/c mice treated with MC26-LucF cells, as determined by colony counts (mean ± SEM; $n = 5$ each).

Engineered PROP-Z maintain plasmid expression and function over time

Synthetic gene circuits are often constructed on intracellular plasmids, which function well in the short term (Fig. 5A) but lose stability and function in stringent conditions such as those found in the tumor microenvironment (*15*, *42*). To design synthetic gene circuits suitable for use over prolonged periods, we engineered a dual-maintenance vector to ensure the long-term stability of our PROP platform (Fig. 5B). The first maintenance device is a toxin-antitoxin system that simultaneously produces a toxin (hok) and a short-lived antitoxin (sok), such that in the event of plasmid loss, the cell will be killed by the long-lived toxin (*42*, *43*). The second device, alp7, comes from the *Bacillus subtilis* plasmid, pLS20, and produces filaments that dynamically push plasmids to the poles of the cell, ensuring equal segregation during cell division (*44*). To assay the performance of our maintenance systems, we measured colony counts (±S-Gal) after successive subcultures in vitro, observing nearly complete plasmid maintenance without antibiotics in the presence of both hok and alp7 (Fig. 5C). Additionally, enzymatic lacZ activity remained stable for at least 48 hours (Fig. 5D).

We performed further in vitro experiments under conditions characteristic of the tumor environment, such as low nutrient levels, pH, and oxygen concentrations (*45*, *46*). LacZ activity was generally maintained, though mildly reduced in each stress condition (Fig. 5E and fig. S5). Tumor microenvironments exhibit complex selective pressures that can only be partially modeled in vitro. To rapidly test maintenance constructs and measure colonization over time, we used a subcutaneous cancer model (nude mice, LS174T-LucF colorectal cancer cell line). After intravenous injection and colonization of bacteria, we found that when no stabilization circuits were used, less than 10% of colonized bacteria retained plasmids in the tumors after 24 hours (Fig. 5F). With the addition of the hok/sok maintenance system, 75% of PROP-Z bacteria retained their plasmids for the first 24 hours, followed by a decline to 45% after 72 hours. With the combination of hok/sok and alp7, more than 96% of PROP-Z bacteria remained intact and retained their plasmids after 72 hours in vivo. Although alp7 was the dominant factor, the addition of hok/sok led to a significant increase in maintenance of colonization at 72 hours (fig. S6; $P < 0.05$). This improvement in stability likely results from the combination of pre- and postdivision mechanisms that promote plasmid maintenance, mirroring natural strategies used by bacteria (*43*). This fully stabilized, high-copy expression vector may prove advantageous for other in vivo applications.

PROP-Z–colonized tumors exhibit increased lacZ activity over time

Having established that orally delivered PROP-Z can specifically, sensitively, and stably colonize experimental liver metastases, we next sought to adapt this platform for use in metastasis detection. The basis of using PROP-Z for noninvasive detection of tumor metastases depends on their capacity to activate a systemically administered agent, the product of which will be both excreted and detectable in the urine (Fig. 1). To quantify the degree of amplification achieved by our diagnostic, we first performed a proof-of-concept study by colonizing subcutaneous tumors (nude mice, LS174T-LucF cell line) with intravenous injections of PROP-Z containing both of the plasmid maintenance tools described above. We then excised and homogenized colonized subcutaneous tumors over the course of 3 days and performed colorimetric assays for lacZ activity [chlorophenol red-ß-D-galactopyranoside (CPRG) assay] at each time point. After 3 days, we observed a nearly five times enhanced lacZ-dependent signal compared to tumors with no bacteria (Fig. 6A).

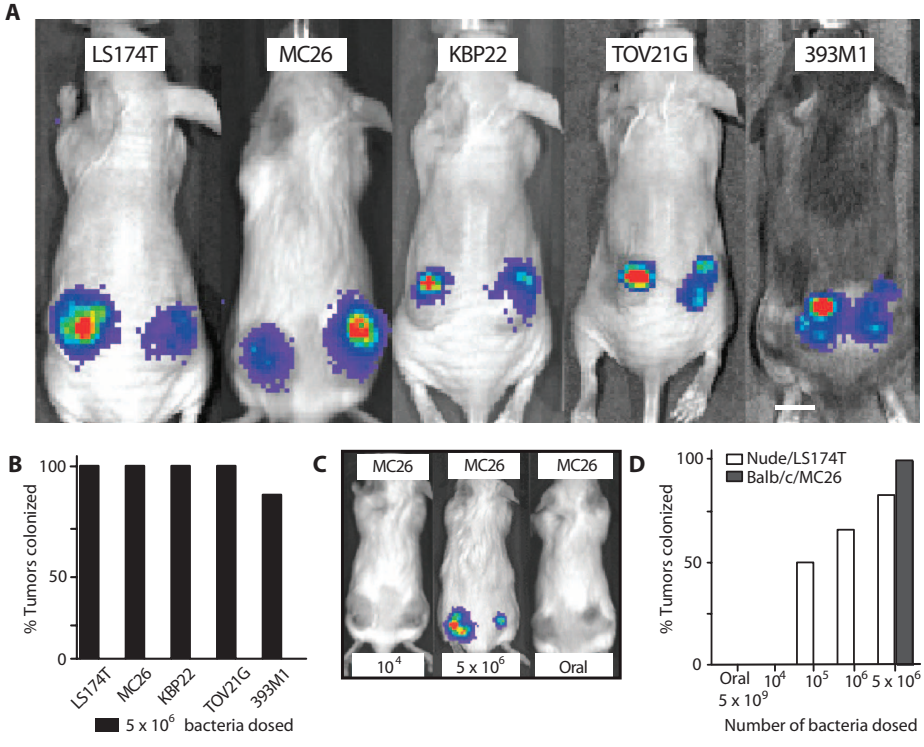

Fig. 4. Colonization in tumor models and different modes of administration. (**A**) IVIS images showing colonization of subcutaneous human (LS174T-LucF, TOV21G) or mouse (MC26, KBP22, 393M1-LucF) tumors by 5×10^6 CFU PROP-Z, 1 to 3 days after intravenous administration to immunocompetent mice. (**B**) Colonization was determined by observing flank luminescence from bacteria 1 to 3 days after bacteria administration using IVIS and is expressed as % tumors colonized. $n = 6$ tumors per cell line. (**C**) IVIS images of mice (MC26-LucF:Balb/c) intravenously injected with 10^4 or 5×10^6 CFU PROP-Z or administered with 5×10^9 CFU PROP-Z via oral gavage. (**D**) Colonization determined in two models upon oral (5×10^9) or intravenous (10^4 to 5×10^6) injection of PROP-Z and expressed as % colonized. $n = 6$ tumors per dosage.

PROP-Z detects liver metastases via the urine with high specificity and sensitivity

To test the potential of our platform to serve as a urine diagnostic, we orally delivered PROP-Z or lacZ-deficient bacteria to immunocompetent mice bearing MC26-LucF liver metastases. We also administered LuGal, a soluble conjugate of luciferin and galactose. Here, PROP-Z bacteria can use lacZ activity to convert this substrate to luciferin, which can be readily detected in the urine using a luciferase assay

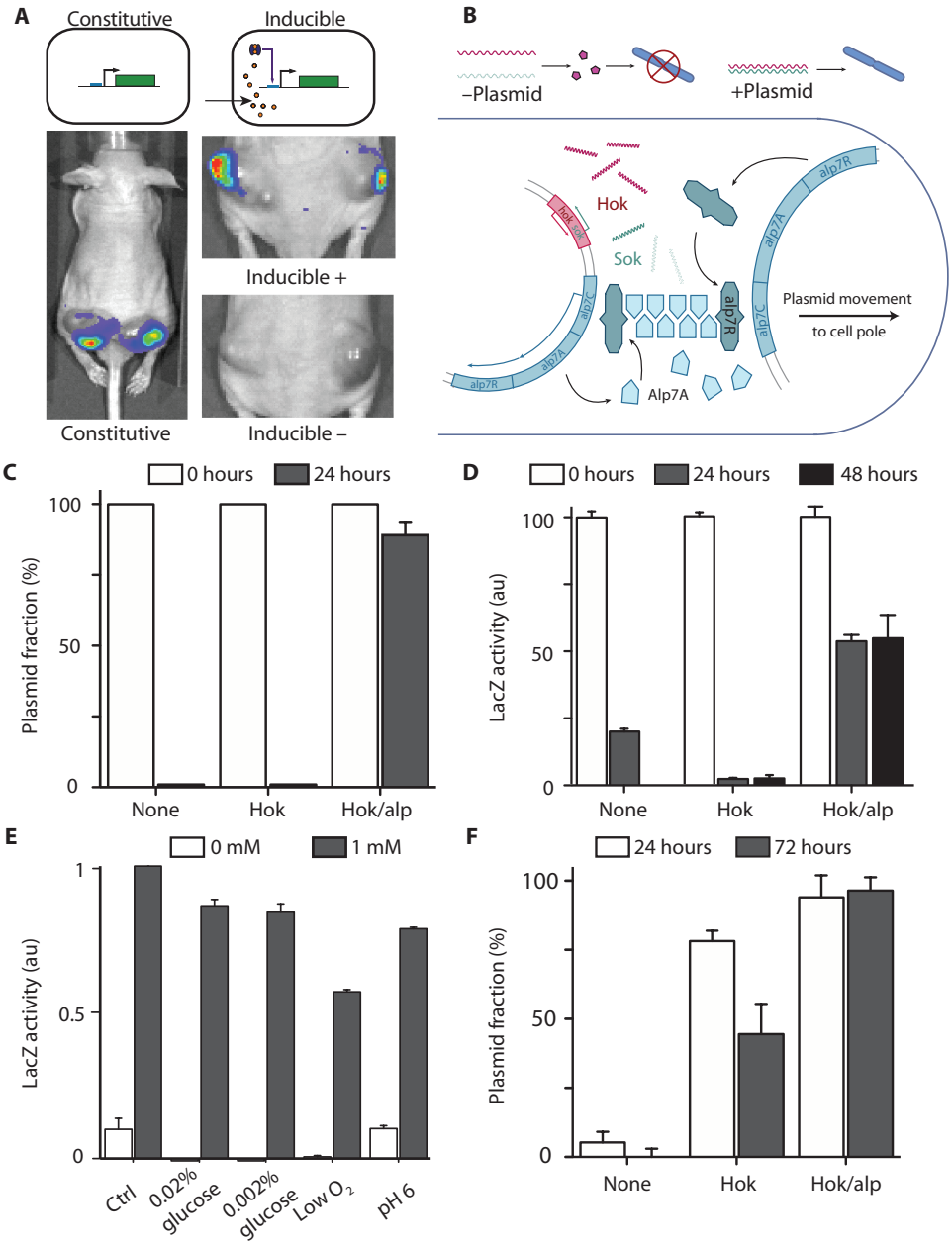

Fig. 5. Dually stabilized vector efficiently maintains PROP-Z activity in vivo. (**A**) Bacteria luciferase signals from a constitutive luxCDABE circuit (PROP-Luc) or an AHL-inducible luxCDABE circuit (PROPi-Luc) 24 hours after bacterial intravenous injection. (**B**) The dual-stabilized maintenance system ensures plasmid stability in the tumor environment. (**C** and **D**) Bacteria were grown overnight with antibiotics (0 hours), and then subcultured without antibiotics and assayed for persistence of the lacZ plasmid by performing differential colony counts (black/white colonies on LB S-Gal plates) (see Materials and Methods) (C) and by assaying for lacZ enzymatic activity (D). au, arbitrary unit. Mean ± SEM; $n = 4$. (**E**) LacZ activity was assayed under reduced nutrient (glucose from 0.02 to 0.002%), pH, and oxygen in the presence of the lacZ inducer (1 mm of IPTG) or in noninducing conditions (0 mM). (**F**) The plasmid was measured after intravenous delivery of bacteria in a subcutaneous cancer model (LS174T-LucF, nude mice). Tumors were analyzed by colony counts on either plasmid-selective (kanamycin + erythromycin) or non–plasmid-selective plates (erythromycin only). Mean ± SEM; $n = 5$.

kit. After tumor colonization, LuGal was administered intravenously, followed by urine collection. Testing as little as 1 μl of the collected urine was sufficient to elicit a positive luciferase signal, which derives from lacZ-mediated cleavage of LuGal to release luciferin into circulation, and the subsequent clearance of this product by the kidney. Thus, we were able to detect the presence of metastatic tumors within 24 hours of oral PROP-Z administration.

In quantifying the performance by our diagnostic across multiple replicates of control models including healthy mice and administration of lacZ-negative bacteria (Fig. 6B), we measured a total in vivo signal-to-noise ratio (SNR) of about 3.6 when comparing the average luciferase signal yielded by PROP-Z–colonized liver metastases to control PROP-Z–treated animals that did not bear tumors. This SNR was sufficient for intravenously administered CPRG substrate to achieve readily visible urinary color changes in test cases (Fig. 6B, inset). As further evidence of robust diagnostic performance, we observed consistent increases in urine luciferase measurements over time in individual mice, demonstrating growth of colonized PROP-Z in the entire cohort (Fig. 6C). Acquiring a baseline, premeasurement value allows for the calculation of signal ratios using the ratio of readings taken from day 1 to day 0. Use of these values greatly reduces the coefficient of variance (CV) between our data sets and allows for more accurate quantitation of our diagnostic (CV = 0.6 to 0.75 versus CV = 0.32 for the ratios; Fig. 6, B and C). Our diagnostic performed similarly in tumors established with several cell lines, including a second liver metastasis model derived from a GEMM cell line (393M1-LucF). In this setting, we quantified an in vivo diagnostic SNR of 4.6, a value similar to that measured in our syngeneic colorectal tumor hosts, indicating that diagnostic performance can be generalized across multiple models (Fig. 6D). Furthermore, we also observed a consistent increase in signal output when comparing individuals on day 1 versus day 2 in the 393M1-LucF model, supporting the potential capacity of PROP-Z to monitor tumor burden as a function of time (Fig. 6D). We additionally demonstrated no significant signal resulting from a mock surgery [phosphate-buffered saline (PBS) was injected instead of metastasis-forming 393M1 cells] to control for any diagnostic signal that might have arisen in response to any surgical trauma required to establish the tumor model (Fig. 6E). The specificity of the SNR in the two liver metastasis models was further supported by our failure to detect any significant correlation in urine signals produced after PROP-Z were delivered to control or liver-damaged mice in a

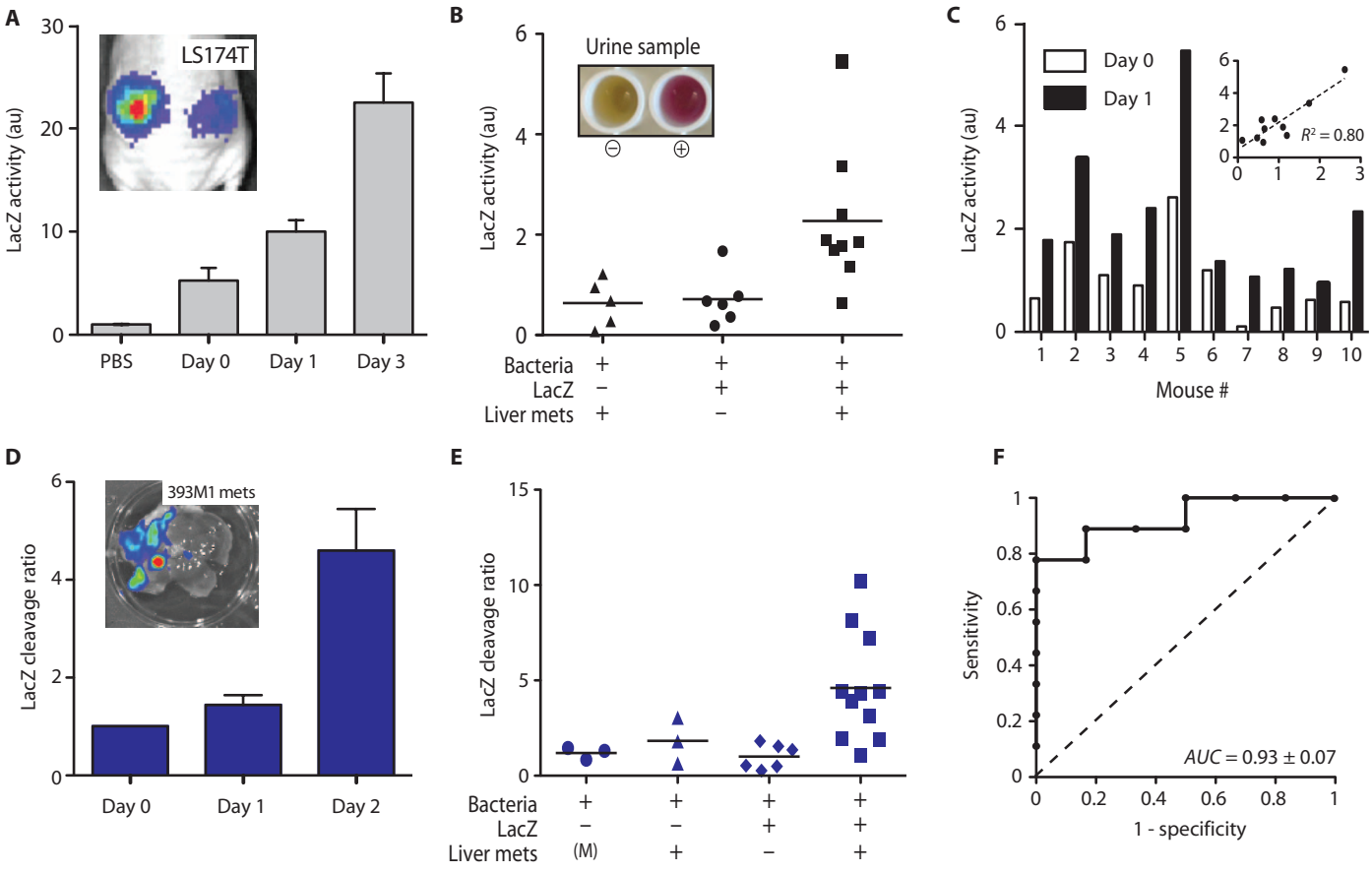

Fig. 6. Detection of metastatic tumors by PROP-Z urine diagnostic. (**A**) Subcutaneous tumor homogenates (nude mice, LS174T-LucF cell line) were analyzed for lacZ activity on days 0, 1, and 3 after intravenous injection of 5×10^6 CFU of PROP-Z bacteria (mean ± SEM; $n = 5$ each). (**B**) PROP-Z activity was quantified after systemic injection of LuGal, a lacZ substrate that when cleaved produces luciferin, which is measured with a subsequent urine assay for luminescence (mean ± SEM; $n = 5$, 6, and 9). $P < 0.05$ Student's t test for the +bacteria/+liver metastasis/+lacZ case against the other two cases. (Inset) Representative cleavage assay using a color change substrate (CPRG) for the PROP-Z–treated mice either with or without liver metastases. (**C**) Paired measurements taken on days 0 and 1 after PROP-Z administered by gavage in individual mice. (Inset) Correlation of luciferase values on days 0 and 1 for each of the $n = 10$ mice in the cohort. (**D**) LacZ cleavage ratios shown for the 393M1-LucF liver metastasis model. Mean values ± SEM. $P < 0.0001$, one-way analysis of variance (ANOVA), Bonferroni post-test resulting in significant ($P < 0.05$) differences between day 0 versus day 2 and day 1 versus day 2. (Inset) IVIS image showing bacterial colonization of liver metastasis. (**E**) Urine assay lacZ cleavage data obtained after PROP-Z oral delivery to test animals (+liver metastasis, +PROP-Z), two cohorts of control mice [(M) mock surgery with PBS injected instead of PROP-Z; +liver metastases, +PROP–non-lacZ], and healthy mice (–liver metastases, +PROP-Z). (**F**) Receiver operating characteristic (ROC) plot illustrates the performance of a binary classifier system as the threshold is varied between case (+LM) and control (–LM) groups in data for (B). The area under the curve (AUC = 0.93) is a metric that characterizes the predictive power of the candidate diagnostic under these specific conditions.

DDC-induced fibrosis model ($P = 0.9$, Student's t test; $n = 4$ mice per group).

The most critical aspects of any diagnostic technology are its sensitivity and specificity (*47*–*49*). To quantify the performance of our diagnostic, we performed a ROC analysis to compare the two most relevant treatment groups in our MC26-LucF model (oral delivery of PROP-Z to mice with or without liver metastases; data from Fig. 6B) (Fig. 6F). The ROC curve illustrates the performance of a binary classifier system as the threshold is varied between case and control groups, and is used as the clinical standard for determining the performance of candidate diagnostics. To characterize the predictive power of a diagnostic, typically, the AUC (area under curve) is used as a metric, such that candidate biomarkers that achieve a baseline AUC value of 0.5 are considered no more predictive than a random biomarker, whereas an AUC score of 1 represents a perfect diagnostic. Our PROP-Z models yield an AUC of 0.93, which is indicative of relatively low false-negative and false-positive rates for our tested model. Furthermore, by using the day 1/day 0 ratio (from Fig. 6C) as a diagnostic value, we found not only a significant reduction in variability but also an enhancement in the AUC (=1.0). The PROP-Z platform can achieve high sensitivity via signal amplification resulting from bacterial growth, high enzyme production from stable plasmids, and enzymatic turnover. Although traditional diagnostics are constrained by the limited fraction of the injected dose that reaches the site of interest (*50*), even small numbers of PROP-Z bacteria that colonize a tumor will quickly expand enough to amplify the signal, allowing for a detectable value that rises above the inherent in vivo background cleavage levels (fig. S7).

DISCUSSION

We have developed a probiotic microbial diagnostic that can sensitively, specifically, and safely detect the presence of hepatic tumors in two models of liver metastasis. Oral delivery of PROP-Z generated a high-contrast urine signal through selective expansion of the probiotic in liver metastases. Furthermore, we established that EcN, used in our PROP platform, was safe, based on its lack of colonization of healthy organs or fibrotic liver tissue and the fact that we noted no deleterious health effects on mice for more than 12 months after oral delivery. Our data suggest that the colonization of tumors is dose-dependent. Nevertheless, the natural reticuloendothelial filtration of gut-derived venous outflow by the liver maximizes liver exposure to gut bacteria, and thus, orally delivered microbes selectively colonize liver metastases (*38*, *51*–*53*).

Early detection of liver metastasis is a pressing clinical need. Liver cancer is prevalent and is difficult to detect with conventional imaging because of poor tumor-to-organ contrast. Our technology may be useful for detection of primary hepatocellular carcinoma in patients at risk for malignant transformation (for example, chronic viral hepatitis). Tumors in other organs that are exposed to high bacterial concentrations from the gastrointestinal tract, such as colorectal cancers, may also be amenable to detection with our PROP platform.

The safety of attenuated *S. typhimurium* bacteria has been demonstrated in clinical trials (*9*), although this finding has not yet been extended to oral delivery and engineered microbes. Here, we chose a host strain, EcN, which has been prescribed in humans and has an established safety record in clinical trials for oral delivery to gastrointestinal disorders (*54*). One advantage in using bacterial diagnostics is their susceptibility to antibiotics, which can be administered to eliminate the agent (*41*).

Moving forward, there are many issues that must be addressed as clinical translation of the PROP platform is considered. For example, the selective trafficking of oral PROP to translocate across the gut wall and colonize liver lesions relative to the preexisting gut microbiome must be investigated in humans because of the many species-specific differences between rodents and man. Additionally, in light of emerging evidence of endogenous tumor microbiomes that vary with site of disease (*3*, *55*), the interaction of bacterial species must be examined. Special attention must also be paid to the fate of PROP in patients who are undergoing therapy that may have immunomodulatory effects (for example, radiation, cytotoxic chemotherapy, and immunotherapy). Another potential concern is interference of PROP or the resultant inflammatory response with radiographic imaging or positron emission tomography surveillance studies. Last, any approach using engineered bacterial species in patients will require regulatory approval before becoming a clinical reality. In this regard, the regulatory landscape that is being established for fecal transplantation will be beneficial (*56*).

Joining a list of recent next-generation diagnostics (circulating tumor cell assays, biomarker monitoring), PROP aims to build toward early identification of micrometastatic disease that may result in improved patient outcomes and decreased treatment toxicities. With a growing population of patients at risk of developing liver metastases (those who have undergone treatment for primary liver, colorectal, breast, and pancreatic tumors), a highly sensitive, nonsurgical, nonradioactive method for repeated monitoring may be clinically useful. PROP may be amenable to further engineering to allow urinalysis by low-cost paper tests (*57*), additional substrates for colorimetric or MRI-based diagnosis, endoscopic detection, and integration with synthetic biomarkers for cancer (*58*). Ultimately, complex synthetic gene circuits may be extended to therapeutic strategies that use self-triggered gene circuits, such as quorum sensing (*59*) or toggle switches (*60*), to deliver clinical payloads to tumor regions.

MATERIALS AND METHODS

Statistical analyses

Statistical tests were calculated in either Microsoft Excel (Student's *t* test) or GraphPad Prism 5.0 (ANOVA, ROC). The details of the statistical tests carried out are indicated in respective figure legends. Where data were approximately normally distributed, values were compared using either Student's *t* test for single variable or two- or three-way ANOVA. Approximate *P* values were computed for two- or three-way ANOVA (table S2). Mice were randomized in different groups before being assayed.

Animal models

All animal work was approved by the committee on animal care [Massachusetts Institute of Technology (MIT), protocol 0414-022-17]. The liver metastasis model was generated by injecting luciferized mouse cancer cells into surgically externalized spleens of immunocompetent mice (*61*). After 90 s, to allow tumor cells to seed the liver, the spleen was removed to prevent ectopic tumor growth. The two models used were MC26-LucF cell line [Tanabe Laboratory, Massachusetts General Hospital (MGH); injected at 5×10^4 cells per 100 μl of PBS into the spleens of female Balb/c mice 6 weeks of age, Taconic] and 393M1-LucF cell line (Jacks Laboratory, MIT; injected at 1×10^5 cells per 100 μl of PBS into female B6.129SF1/J mice 6 weeks of age, Jackson Laboratory). Animals were monitored via IVIS (IVIS 200, Caliper Life Sciences) for about 3 weeks by intraperitoneal injection of D-luciferin (100 μl, 30 mg/ml, 15-min waiting time) until a radiance value of tumors reached 1×10^9 to 5×10^9 photons $s^{-1}cm^{-2}$ sr^{-1} for the MC26-LucF model or 0.6×10^8 to 3×10^8 photons $s^{-1}cm^{-2}$ sr^{-1} for the 393M1- LucF model. For tumor xenograft models, cancer cell lines were inoculated subcutaneously (0.5×10^7 to 1×10^7 cells per flank) in female mice at 6 weeks of age. In the liver fibrosis model, FVB/NJ mice (Jackson Laboratory) were fed with 0.1% (w/w) DDC (Sigma) or normal rodent chow for 3 weeks (Research Diets), at which point colony counts on extracted livers or urine assays were performed.

Bacterial strains and administration

Plasmid pTKW106alp7A was constructed by adding the 3.5-kb alp7AR cassette from the *B. subtilis* plasmid pLS20 to the pTKW106 lacZ expression vector containing the hok/sok plasmid maintenance system (*42*, *62*). The luxCDABE cassette was genomically integrated into EcN with the p16Slux plasmid (*36*), and subsequently, these bacteria were transformed with the pTKW106alp7A plasmid, creating PROP-Z (Table 1). The plasmid with no stabilizing element (pTKW106_delhok) was created using PCR by removing the hok/sok region of pTKW106. The pTKW106alp7A (alone) plasmid was created using PCR by removing the hok/sok region of pTKW106alp7A. The pTD103luxCDABE plasmid was induced by 10 μM AHL (Sigma-Aldrich). Bacteria were prepared by growth in LB (Sigma-Aldrich) and appropriate antibiotics until exponential phase, washed three times with sterile PBS, and then prepared at the stated concentration in sterile PBS.

IVIS imaging

To image bacterial luminescence from subcutaneous tumors, mice were anesthetized with isoflurane and imaged using an IVIS with an open

filter and auto-exposure setting. Colonization of our liver metastasis model was also observed routinely using IVIS after explantation of livers. For quantification of the tumor size–dependent colonization of liver metastases, we correlated both tumor- and bacteria-derived luminescent signals by IVIS. The bacteria luxCDABE cassette produced a luminescent signal without provision of an exogenous substrate, so bacteria luminescence expression was first measured with an IVIS upon explantation of the liver. Next, livers were soaked in D-luciferin, which generated a luminescent signal derived from MC26-LucF tumors (firefly luciferase). MC26-LucF luciferase gave rise to radiance units of ~1×10^7 to 1×10^{10} photons s^{-1} cm^{-2} sr^{-1}, whereas bacterial-derived luminescence activity led to radiance values in the range of 1×10^5 to 1×10^7 photons s^{-1} cm^{-2} sr^{-1}. This minimal overlap in signal intensities indicated a negligible contribution of bacterial luciferase activity to the readings generated by MC26-LucF luciferase, which allowed for both bacteria luciferase (luxCDABE) and MC26-LucF luciferase (firefly) to be measured sequentially when using an open filter on the IVIS apparatus.

Urine assay

Mice were injected subcutaneously with 1 ml of sterile PBS, followed 1.5 hours later by 100 μl of LuGal (0.5 mg/ml) via tail vein injection. The LuGal injection was immediately followed by a second subcutaneous injection of 1 ml of sterile PBS to promote urine production for retrieval. Mice were placed in urine collection tubes for 1 to 2 hours (*58*). One microliter of urine was tested for luciferin with a luciferase assay kit (Promega QuantiLum Recombinant Luciferase Kit) via luminescence in a Berthold Centro LB 960 reader (measurements done in triplicate). LacZ cleavage values were plotted as the total luciferase activity (the product of luminescence multiplied by the total urine volume collected) with values typically in the range of 5×10^5 to 5×10^6 counts. The inset in Fig. 6B shows an example of the urine diagnostic assay, where CPRG (0.5 mg/ml) was injected intravenously into an animal with high lacZ activity and an observed color change in urine was present (+ label). The control (– label) well represents the CPRG-prompted output of an animal without liver metastases that received oral PROP-Z and thus exhibited very low lacZ cleavage. In all urine experiments, drinking water was supplemented with IPTG at a concentration of 10 mM for the duration of the experiment to induce lacZ expression.

Plasmid stability and β-galactosidase activity in vitro

A strain of an *E. coli* lacZ mutant (Mach One, Invitrogen) was transformed with either pTKW106, pTKW106alp7A, or pTKW106_delhok. Cultures were diluted into LB media (Miller, Sigma-Aldrich) supplemented with antibiotics (kanamycin, 50 μg/ml) and grown until an approximate optical density (OD) = 0.1. Cultures were then subcultured by diluting 1:100 into deep 96-well plates (Corning #3600) with 500 μl of LB without antibiotics and grown for 24 hours. After each 24-hour period, cultures were diluted 1:10,000 and grown again in an additional 96-well plate for 24 hours. β-Galactosidase (lacZ) activity was assessed by supplying a CPRG substrate and measuring absorbance at 575 nm over a 5- to 60-min reading frame using a Tecan i200 plate reader. In wells with more concentrated cultures, wells were diluted from 1 to 10× to achieve a signal that gave rise to a linear absorbance, and the maximum value within this range was recorded as the activity reading for each strain on each day. Plasmid stability was calculated by plating on LB + S-Gal and determining the number of white and black colonies, with the 0-hour time point representing the result from a pre-cultured strain grown with antibiotics. Black colonies indicate positive β-galactosidase activity and hence the presence of the plasmid (*42*). In vitro lacZ activities (Fig. 5D) are normalized to the 0-hour time point for each strain.

Plasmid stability in vivo

Plasmid stability and enzymatic tests were performed in 6-week-old female nude mice (NcrNu strain; Taconic) bearing tumors derived from a human colorectal cancer cell line, LS174T [American Type Culture Collection (ATCC)], that harbor a firefly luciferase transgene (LS174T_LucF, Table 1). Tumors were initiated by subcutaneous injection of 5×10^6 cells in 100 μl of PBS per flank and grown for 1 to 2 weeks until they reached a size of 5 to 10 mm. To obtain measures of plasmid stability in vivo, EcN-luxCDABE bacteria with pTKW plasmids were injected intravenously at a dosage of 1×10^6 bacteria, and at the designated time point, tumors were sterilely extracted and homogenized using a tissue dissociator (Miltenyi), an aliquot of which was seeded on each of LB erythromcyin (100 μg/ml), and LB erythromycin + kanamycin plates to obtain the percent of bacteria carrying resistant plasmids, or measured for lacZ activity as mentioned above.

Quantification of tumor colonization in subcutaneous models

Colonization of subcutaneous tumors by the PROP-Z strain was determined by IVIS imaging 1 to 3 days after delivery. IVIS signals were used to observe whether a tumor-localized luminescent signal was present, because bacteria express the luxCDABE cassette as a chromosomal integration. Tumors were seeded in each of the models by a subcutaneous injection of 5×10^6 cells per flank and allowed to reach about 3 to 7 mm in size over the course of 2 to 3 weeks. Six tumors were quantified in each case. The human LS174T, KBP22, and TOV21G cells were implanted in nude mice, MC26 cells were implanted in Balb/c mice, and 393M1-LucF lines were implanted in B6.129SF1/J (Jackson), all 6 weeks of age and female. Each of the cell lines were cultured in Eagle's minimum essential medium (EMEM) (LS174T-LucF; from ATCC), RPMI (TOV21G, OVCAR8; from Gibco), or Dulbecco's modified Eagle's medium (DMEM) (KBP22, MC26-LucF, 393M1-LucF; from Cellgro) with 10% fetal bovine serum (Gibco) and 1% penicillin/streptomycin (Corning).

Biodistribution experiments via qPCR and colony counts

After PROP-Z delivery, organs were harvested aseptically using surgical tools treated with a bead sterilizer and washed in ethanol and subsequently in sterile, DNA-free water before use in extracting tissues. A small tissue sample of 10 to 100 mg was excised from each organ and used for DNA isolated with an UltraClean Tissue & Cells DNA Isolation Kit (MoBio). One microliter of DNA sample was used in a subsequent qPCR experiment run according to the manufacturer's parameters (Qiagen, QuantiTect SYBR Kit) on a Bio-Rad iCycler machine. We used specific primers for EcN (Muta 7/8) to quantify PROP-Z levels (*63*). Control curves were run for each qPCR experiment using a known amount of bacteria purified through the UltraClean Tissue & Cells DNA Isolation Kit. Automated C_t values generated from a Bio-Rad iCycler machine exhibit a linear correlation with the known number of bacteria across several orders of magnitude (fig. S3). Colony counts were obtained by excising whole organs, homogenizing in a tissue dissociator (Miltenyi), and plating on erythromycin to specifically detect the presence of EcN/PROP-Z. Comparisons of colony counting from tumors and qPCR experiments were correlated.

MRI quantification of tumor diameters

Mice were imaged using a Varian 7T/310/ASR-whole mouse MRI system (Varian/Agilent). OsiriX software was used to analyze images from liver metastasis–nearing mice by the Koch Institute Animal Imaging and Preclinical Testing staff. Tumor volumes were determined by identifying and enclosing tumors from each slice inside closed polygons, then summating total area for each tumor, and multiplying by the slice thickness to obtain tumor volumes. Tumor diameters were calculated from volumes by assuming spheres [$V = 4/3\ \pi(d/2)^3$].

IVIS quantification of liver metastases

We quantified the area of tumor nodules by visual inspection of the gross pathological specimen and then corroborated the location and size of tumor formation based on the firefly luciferase signal from MC26 cells in IVIS images. Some tumors were not colonized as observed by the presence of the firefly signal in the absence of a bacterial luminescence signal (fig. S2, yellow boxes, center image), but these examples were primarily restricted to the smallest tumors observed (Fig. 2B). Tumor areas were measured and transformed into linear dimensions by assuming $A = \pi(d/2)^2$. The x-axis labels in the histograms represent the center of the bin histograms, that is, tick mark of 2, and indicate tumors in the range of 1.5 to 2.5 mm.

Measuring PROP-Z in whole blood

Blood was collected using a cardiac puncture technique to obtain 500 µl of blood from the animal, diluted immediately in 4.5 ml of PBS, and then plated in the presence of erythromycin for counting of resistant PROP-Z colonies. In our blood count experiments, we orally delivered PROP-Z bacteria to healthy 6-week-old female mice and collected blood at 1, 3, 7, 18, and 24 hours ($n = 3$ per time point), which did not yield any significant colonization via colony counting (detection limit 10^3 CFU per 1 ml of blood, determined by a spiking bacteria into a sterile blood sample). Counts from this positive control and spiked bacteria into PBS were highly correlated.

SUPPLEMENTARY MATERIALS

www.sciencetranslationalmedicine.org/cgi/content/full/7/289/289ra84/DC1
Fig. S1. Map of plasmid pTKW106 alp7A.
Fig. S2. Size and colonization of liver metastases.
Fig. S3. Calibration curve for the qPCR calculation of the number bacteria in a tumor sample.
Fig. S4. Histopathological analysis of organs after oral delivery of PROP-Z.
Fig. S5. Growth and activity of stabilized lacZ plasmid in different oxygen, inducer (IPTG), and antibiotic conditions.
Fig. S6. CFU and stability of constructs in subcutaneous tumor models.
Fig. S7. Background cleavage of LuGal from urine assay.
Table S1. List and quantification of liver metastases.
Table S2. Results of three-way factorial ANOVA.

REFERENCES AND NOTES

1. R. D. Berg, The indigenous gastrointestinal microflora. *Trends Microbiol.* **4**, 430–435 (1996).
2. D. C. Savage, Microbial ecology of the gastrointestinal tract. *Annu. Rev. Microbiol.* **31**, 107–133 (1977).
3. C. Urbaniak, J. Cummins, M. Brackstone, J. M. Macklaim, G. B. Gloor, C. K. Baban, L. Scott, D. M. O'Hanlon, J. P. Burton, K. P. Francis, M. Tangney, G. Reid, Microbiota of human breast tissue. *Appl. Environ. Microbiol.* **80**, 3007–3014 (2014).
4. L. Yang, X. Lu, C. W. Nossa, F. Francois, R. M. Peek, Z. Pei, Inflammation and intestinal metaplasia of the distal esophagus are associated with alterations in the microbiome. *Gastroenterology* **137**, 588–597 (2009).
5. W. B. Coley, The treatment of malignant tumors by repeated inoculations of erysipelas. With a report of ten original cases. *Clin. Orthop. Relat. Res.* 3–11 (1893).
6. N. S. Forbes, Engineering the perfect (bacterial) cancer therapy. *Nat. Rev. Cancer* **10**, 785–794 (2010).
7. S. Xiang, J. Fruehauf, C. J. Li, Short hairpin RNA–expressing bacteria elicit RNA interference in mammals. *Nat. Biotechnol.* **24**, 697–702 (2006).
8. M. Zhao, M. Yang, X.-M. Li, P. Jiang, E. Baranov, S. Li, M. Xu, S. Penman, R. M. Hoffman, Tumor-targeting bacterial therapy with amino acid auxotrophs of GFP-expressing *Salmonella typhimurium*. *Proc. Natl. Acad. Sci. U.S.A.* **102**, 755–760 (2005).
9. J. F. Toso, V. J. Gill, P. Hwu, F. M. Marincola, N. P. Restifo, D. J. Schwartzentruber, R. M. Sherry, S. L. Topalian, J. C. Yang, F. Stock, L. J. Freezer, K. E. Morton, C. Seipp, L. Haworth, S. Mavroukakis, D. White, S. MacDonald, J. Mao, M. Sznol, S. A. Rosenberg, Phase I study of the intravenous administration of attenuated *Salmonella typhimurium* to patients with metastatic melanoma. *J. Clin. Oncol.* **20**, 142–152 (2002).
10. P. Brader, J. Stritzker, C. C. Riedl, P. Zanzonico, S. Cai, E. M. Burnazi, E. R. Ghani, H. Hricak, A. A. Szalay, Y. Fong, R. Blasberg, *Escherichia coli* Nissle 1917 facilitates tumor detection by positron emission tomography and optical imaging. *Clin. Cancer Res.* **14**, 2295–2302 (2008).
11. S. A. Soghomonyan, M. Doubrovin, J. Pike, X. Luo, M. Ittensohn, J. D. Runyan, J. Balatoni, R. Finn, J. G. Tjuvajev, R. Blasberg, D. Bermudes, Positron emission tomography (PET) imaging of tumor-localized *Salmonella* expressing HSV1-TK. *Cancer Gene Ther.* **12**, 101–108 (2005).
12. J. Stritzker, S. Weibel, P. J. Hill, T. A. Oelschlaeger, W. Goebel, A. A. Szalay, Tumor-specific colonization, tissue distribution, and gene induction by probiotic *Escherichia coli* Nissle 1917 in live mice. *Int. J. Med. Microbiol.* **297**, 151–162 (2007).
13. Y. A. Yu, S. Shabahang, T. M. Timiryasova, Q. Zhang, R. Beltz, I. Gentschev, W. Goebel, A. A. Szalay, Visualization of tumors and metastases in live animals with bacteria and vaccinia virus encoding light-emitting proteins. *Nat. Biotechnol.* **22**, 313–320 (2004).
14. M. Cronin, D. Morrissey, S. Rajendran, S. M. El Mashad, D. van Sinderen, G. C. O'Sullivan, M. Tangney, Orally administered bifidobacteria as vehicles for delivery of agents to systemic tumors. *Mol. Ther.* **18**, 1397–1407 (2010).
15. T. Danino, J. Lo, A. Prindle, J. Hasty, S. N. Bhatia, In vivo gene expression dynamics of tumor-targeted bacteria. *ACS Synth. Biol.* **1**, 465–470 (2012).
16. A. Prindle, J. Selimkhanov, T. Danino, P. Samayoa, A. Goldberg, S. N. Bhatia, J. Hasty, Genetic circuits in *Salmonella typhimurium*. *ACS Synth. Biol.* **1**, 458–464 (2012).
17. A. Prindle, P. Samayoa, I. Razinkov, T. Danino, L. S. Tsimring, J. Hasty, A sensing array of radically coupled genetic 'biopixels'. *Nature* **481**, 39–44 (2012).
18. A. Prindle, J. Selimkhanov, H. Li, I. Razinkov, L. S. Tsimring, J. Hasty, Rapid and tunable post-translational coupling of genetic circuits. *Nature* **508**, 387–391 (2014).
19. J. J. Tabor, H. M. Salis, Z. B. Simpson, A. A. Chevalier, A. Levskaya, E. M. Marcotte, C. A. Voigt, A. D. Ellington, A synthetic genetic edge detection program. *Cell* **137**, 1272–1281 (2009).
20. T. Danino, O. Mondragón-Palomino, L. Tsimring, J. Hasty, A synchronized quorum of genetic clocks. *Nature* **463**, 326–330 (2010).
21. A. E. Friedland, T. K. Lu, X. Wang, D. Shi, G. Church, J. J. Collins, Synthetic gene networks that count. *Science* **324**, 1199–1202 (2009).
22. M. Elowitz, S. Leibler, A synthetic oscillatory network of transcriptional regulators. *Nature* **403**, 335–338 (2000).
23. T. S. Gardner, C. R. Cantor, J. J. Collins, Construction of a genetic toggle switch in *Escherichia coli*. *Nature* **403**, 339–342 (2000).
24. T. K. Lu, J. J. Collins, Engineered bacteriophage targeting gene networks as adjuvants for antibiotic therapy. *Proc. Natl. Acad. Sci. U.S.A.* **106**, 4629–4634 (2009).
25. F. Duan, K. L. Curtis, J. C. March, Secretion of insulinotropic proteins by commensal bacteria: Rewiring the gut to treat diabetes. *Appl. Environ. Microbiol.* **74**, 7437–7438 (2008).
26. S. Rao, S. Hu, L. McHugh, K. Lueders, K. Henry, Q. Zhao, R. A. Fekete, S. Kar, S. Adhya, D. H. Hamer, Toward a live microbial microbicide for HIV: Commensal bacteria secreting an HIV fusion inhibitor peptide. *Proc. Natl. Acad. Sci. U.S.A.* **102**, 11993–11998 (2005).
27. F. Duan, J. C. March, Engineered bacterial communication prevents *Vibrio cholerae* virulence in an infant mouse model. *Proc. Natl. Acad. Sci. U.S.A.* **107**, 11260–11264 (2010).
28. D. M. Heimann, S. A. Rosenberg, Continuous intravenous administration of live genetically modified *Salmonella typhimurium* in patients with metastatic melanoma. *J. Immunother.* **26**, 179–180 (2003).
29. J. Nemunaitis, C. Cunningham, N. Senzer, J. Kuhn, J. Cramm, C. Litz, R. Cavagnolo, A. Cahill, C. Clairmont, M. Sznol, Pilot trial of genetically modified, attenuated Salmonella expressing the *E. coli cytosine* deaminase gene in refractory cancer patients. *Cancer Gene Ther.* **10**, 737–744 (2003).
30. A. Schroeder, D. A. Heller, M. M. Winslow, J. E. Dahlman, G. W. Pratt, R. Langer, T. Jacks, D. G. Anderson, Treating metastatic cancer with nanotechnology. *Nat. Rev. Cancer* **12**, 39–50 (2011).
31. K. R. Hess, G. R. Varadhachary, S. H. Taylor, W. Wei, M. N. Raber, R. Lenzi, J. L. Abbruzzese, Metastatic patterns in adenocarcinoma. *Cancer* **106**, 1624–1633 (2006).
32. P. M. Lykoudis, D. O'Reilly, K. Nastos, G. Fusai, Systematic review of surgical management of synchronous colorectal liver metastases. *Br. J. Surg.* **101**, 605–612 (2014).

33. L. C. Cummings, J. D. Payes, G. S. Cooper, Survival after hepatic resection in metastatic colorectal cancer: A population-based study. *Cancer* **109**, 718–726 (2007).
34. S. A. Shah, R. Bromberg, A. Coates, E. Rempel, M. Simunovic, S. Gallinger, Survival after liver resection for metastatic colorectal carcinoma in a large population. *J. Am. Coll. Surg.* **205**, 676–683 (2007).
35. K. E. Rusthoven, B. D. Kavanagh, H. Cardenes, V. W. Stieber, S. H. Burri, S. J. Feigenberg, M. A. Chidel, T. J. Pugh, W. Franklin, M. Kane, L. E. Gaspar, T. E. Schefter, Multi-institutional phase I/II trial of stereotactic body radiation therapy for liver metastases. *J. Clin. Oncol.* **27**, 1572–1578 (2009).
36. C. U. Riedel, P. G. Casey, H. Mulcahy, F. O'Gara, C. G. Gahan, C. Hill, Construction of p16*Slux*, a novel vector for improved bioluminescent labeling of gram-negative bacteria. *Appl. Environ. Microbiol.* **73**, 7092–7095 (2007).
37. E. A. Meighen, Molecular biology of bacterial bioluminescence. *Microbiol. Rev.* **55**, 123–142 (1991).
38. N. Kaplowitz, *Liver and Biliary Diseases* (Williams & Wilkins, Baltimore, MD, 1996).
39. P. Fickert, U. Stöger, A. Fuchsbichler, T. Moustafa, H. U. Marschall, A. H. Weiglein, O. Tsybrovskyy, H. Jaeschke, K. Zatloukal, H. Denk, M. Trauner, A new xenobiotic-induced mouse model of sclerosing cholangitis and biliary fibrosis. *Am. J. Pathol.* **171**, 525–536 (2007).
40. M. M. Winslow, T. L. Dayton, R. G. Verhaak, C. Kim-Kiselak, E. L. Snyder, D. M. Feldser, D. D. Hubbard, M. J. DuPage, C. A. Whittaker, S. Hoersch, S. Yoon, D. Crowley, R. T. Bronson, D. Y. Chiang, M. Meyerson, T. Jacks, Suppression of lung adenocarcinoma progression by Nkx2-1. *Nature* **473**, 101–104 (2011).
41. N. J. Roberts, L. Zhang, F. Janku, A. Collins, R. Y. Bai, V. Staedtke, A. W. Rusk, D. Tung, M. Miller, J. Roix, K. V. Khanna, R. Murthy, R. S. Benjamin, T. Helgason, A. D. Szvalb, J. E. Bird, S. Roy-Chowdhuri, H. H. Zhang, Y. Qiao, B. Karim, J. McDaniel, A. Elpiner, A. Sahora, J. Lachowicz, B. Phillips, A. Turner, M. K. Klein, G. Post, L. A. Diaz Jr., G. J. Riggins, N. Papadopoulos, K. W. Kinzler, B. Vogelstein, C. Bettegowda, D. L. Huso, M. Varterasian, S. Saha, S. Zhou, Intratumoral injection of *Clostridium novyi*-NT spores induces antitumor responses. *Sci. Transl. Med.* **6**, 249ra111 (2014).
42. T. K. Wood, R. H. Kuhn, S. W. Peretti, Enhanced plasmid stability through post-segregational killing of plasmid-free cells. *Biotechnol. Tech.* **4**, 39–44 (1990).
43. K. Gerdes, The *parB* (*hok/sok*) locus of plasmid R1: A general purpose plasmid stabilization system. *Nat. Biotechnol.* **6**, 1402–1405 (1988).
44. A. I. Derman, E. C. Becker, B. D. Truong, A. Fujioka, T. M. Tucey, M. L. Erb, P. C. Patterson, J. Pogliano, Phylogenetic analysis identifies many uncharacterized actin-like proteins (Alps) in bacteria: Regulated polymerization, dynamic instability and treadmilling in Alp7A. *Mol. Microbiol.* **73**, 534–552 (2009).
45. G. Helmlinger, F. Yuan, M. Dellian, R. K. Jain, Interstitial pH and pO_2 gradients in solid tumors in vivo: High-resolution measurements reveal a lack of correlation. *Nat. Med.* **3**, 177–182 (1997).
46. P. Vaupel, F. Kallinowski, P. Okunieff, Blood flow, oxygen and nutrient supply, and metabolic microenvironment of human tumors: A review. *Cancer Res.* **49**, 6449–6465 (1989).
47. P. Yager, G. J. Domingo, J. Gerdes, Point-of-care diagnostics for global health. *Annu. Rev. Biomed. Eng.* **10**, 107–144 (2008).
48. M. Carpelan-Holmström, J. Louhimo, U. H. Stenman, H. Alfthan, H. Järvinen, C. Haglund, Estimating the probability of cancer with several tumor markers in patients with colorectal disease. *Oncology* **66**, 296–302 (2004).
49. V. Kulasingam, Y. Zheng, A. Soosaipillai, A. E. Leon, M. Gion, E. P. Diamandis, Activated leukocyte cell adhesion molecule: A novel biomarker for breast cancer. *Int. J. Cancer* **125**, 9–14 (2009).
50. E. Ruoslahti, S. N. Bhatia, M. J. Sailor, Targeting of drugs and nanoparticles to tumors. *J. Cell Biol.* **188**, 759–768 (2010).
51. M. A. Herman, D. Fromm, D. Kessel, Tumor blood-flow changes following protoporphyrin IX-based photodynamic therapy in mice and humans. *J. Photochem. Photobiol. B* **52**, 99–104 (1999).
52. B. Davies, T. Morris, Physiological parameters in laboratory animals and humans. *Pharm. Res.* **10**, 1093–1095 (1993).
53. M. L. Balmer, E. Slack, A. de Gottardi, M. A. Lawson, S. Hapfelmeier, L. Miele, A. Grieco, H. Van Vlierberghe, R. Fahrner, N. Patuto, C. Bernsmeier, F. Ronchi, M. Wyss, D. Stroka, N. Dickgreber, M. H. Heim, K. D. McCoy, A. J. Macpherson, The liver may act as a firewall mediating mutualism between the host and its gut commensal microbiota. *Sci. Transl. Med.* **6**, 237ra66 (2014).
54. M. Schultz, Clinical use of *E. coli* Nissle 1917 in inflammatory bowel disease. *Inflamm. Bowel Dis.* **14**, 1012–1018 (2008).
55. J. Cummins, M. Tangney, Bacteria and tumours: Causative agents or opportunistic inhabitants? *Infect. Agent. Cancer* **8**, 11 (2013).
56. A. D. Kostic, R. J. Xavier, D. Gevers, The microbiome in inflammatory bowel disease: Current status and the future ahead. *Gastroenterology* **146**, 1489–1499 (2014).
57. A. D. Warren, G. A. Kwong, D. K. Wood, K. Y. Lin, S. N. Bhatia, Point-of-care diagnostics for noncommunicable diseases using synthetic urinary biomarkers and paper microfluidics. *Proc. Natl. Acad. Sci. U.S.A.* **111**, 3671–3676 (2014).
58. G. A. Kwong, G. von Maltzahn, G. Murugappan, O. Abudayyeh, S. Mo, I. A. Papayannopoulos, D. Y. Sverdlov, S. B. Liu, A. D. Warren, Y. Popov, D. Schuppan, S. N. Bhatia, Mass-encoded synthetic biomarkers for multiplexed urinary monitoring of disease. *Nat. Biotechnol.* **31**, 63–70 (2013).
59. C. A. Swofford, N. Van Dessel, N. S. Forbes, Quorum-sensing *Salmonella* selectively trigger protein expression within tumors. *Proc. Natl. Acad. Sci. U.S.A.* **112**, 3457–3462 (2015).
60. J. W. Kotula, S. J. Kerns, L. A. Shaket, L. Siraj, J. J. Collins, J. C. Way, P. A. Silver, Programmable bacteria detect and record an environmental signal in the mammalian gut. *Proc. Natl. Acad. Sci. U.S.A.* **111**, 4838–4843 (2014).
61. K. C. Soares, K. Foley, K. Olino, A. Leubner, S. C. Mayo, A. Jain, E. Jaffee, R. D. Schulick, K. Yoshimura, B. Edil, L. Zheng, A preclinical murine model of hepatic metastases. *J. Vis. Exp.* **27**, e51677 (2014).
62. K. Wu, T. K. Wood, Evaluation of the *hok/sok* killer locus for enhanced plasmid stability. *Biotechnol. Bioeng.* **44**, 912–921 (1994).
63. G. Blum-Oehler, S. Oswald, K. Eiteljörge, U. Sonnenborn, J. Schulze, W. Kruis, J. Hacker, Development of strain-specific PCR reactions for the detection of the probiotic *Escherichia coli* strain Nissle 1917 in fecal samples. *Res. Microbiol.* **154**, 59–66 (2013).

Acknowledgments: We thank J. Voog and members of the Bhatia laboratory for the helpful discussions and H. Fleming for the critical reading and editing of the manuscript. K. Tanabe and B. Fuchs (MGH) provided the luciferized MC26 cell line (MC26-LucF). We thank the Koch Institute Swanson Biotechnology Center for technical support, specifically S. Malstrom in the Koch Institute Animal Imaging and Preclinical Testing core, as well as the Koch Institute Histology Core. We thank H. Ding of The Barbara K. Ostrom (1978) Bioinformatics and Computing Facility in the Swanson Biotechnology Center. **Funding:** This work was supported in part by the Ludwig Center for Molecular Oncology at MIT, an Amar G. Bose Research Grant, The San Diego Center for Systems Biology (NIH grant P50 GM085764), the National Institutes of Health and General Medicine (R01GM69811), the Koch Institute Support (core) grant P30-CA14051 from the National Cancer Institute, and a Core Center Grant P30-ES002109 from the National Institute of Environmental Health Sciences. This work was additionally supported by Misrock and National Research Service Awards Postdoctoral Fellowships (T.D.), National Defense Science and Engineering Graduate Fellowship (A.P.), and Career Award at the Scientific Interface from the Burroughs Wellcome Fund (G.A.K.). S.N.B. is a Howard Hughes Medical Institute investigator. **Author contributions:** T.D., A.P., M.S., K.A., and G.A.K. performed the experiments. T.D., A.P., M.S., K.A., G.K., S.N.B., and J.H. designed the experiments. All authors and H. Fleming wrote and edited the manuscript. **Competing interests:** S.N.B. is a co-founder of and on the Scientific Advisory Board of Hepregen and a co-founder of Zymera. The other authors declare that they have no competing interests. MIT has filed a patent on diagnostic programmable probiotics, based in part on the work reported here. **Data and materials availability:** The pTKW106alpA plasmid and variants are available upon request through a material transfer agreement.

Submitted 24 November 2014
Accepted 31 March 2015
Published 27 May 2015
10.1126/scitranslmed.aaa3519

Citation: T. Danino, A. Prindle, G. A. Kwong, M. Skalak, H. Li, K. Allen, J. Hasty, S. N. Bhatia, Programmable probiotics for detection of cancer in urine. *Sci. Transl. Med.* **7**, 289ra84 (2015).

Science Translational Medicine AAAS

Programmable probiotics for detection of cancer in urine
Tal Danino *et al.*
Sci Transl Med **7**, 289ra84 (2015);
DOI: 10.1126/scitranslmed.aaa3519

Editor's Summary

Synthetic bacteria for tumor detection

Tumors often harbor bacteria, and Danino *et al.* have taken advantage of this peculiar fact to design a method to detect liver metastases. An *E. coli* strain was carefully engineered to carry β-galactosidase, an enzyme that can metabolize numerous substrates. When fed to mice, these bacteria transited the gut epithelium to enter the bloodstream and then traveled to the liver, where they take up residence in any tumor colonies that are present. At that point, the mice were fed LuGal, a combined luciferin and galactose molecule. When the LuGal reached the bacteria in the tumors, the bacterial β-galactosidase metabolized it to luciferin, which was then excreted in the urine. The amount of luciferin, an easily detectible molecule, revealed the tumor burden carried in the liver. It remains to be seen whether this noninvasive approach to cancer detection can be applied to other tumor types and locations, but the versatility conferred by control of the enzymes in the *E. coli* and the substrates fed to the animal bodes well for future application.

Science Translational Medicine (print ISSN 1946-6234; online ISSN 1946-6242) is published weekly, except the last week in December, by the American Association for the Advancement of Science, 1200 New York Avenue NW, Washington, DC 20005.

www.sciencetranslationalmedicine.org/cgi/content/full/7/289/289ra84/DC1

Supplementary Materials for

Programmable probiotics for detection of cancer in urine

Tal Danino, Arthur Prindle, Gabriel A. Kwong, Matthew Skalak, Howard Li, Kaitlin Allen, Jeff Hasty, Sangeeta N. Bhatia*

*Corresponding author. E-mail: sbhatia@mit.edu

Published 27 May 2015, *Sci. Transl. Med.* **7**, 289ra84 (2015)
DOI: 10.1126/scitranslmed.aaa3519

This PDF file includes:

Other Supplementary Material for this manuscript includes the following:
(available at www.sciencetranslationalmedicine.org/cgi/content/full/7/289/289ra84/DC1)

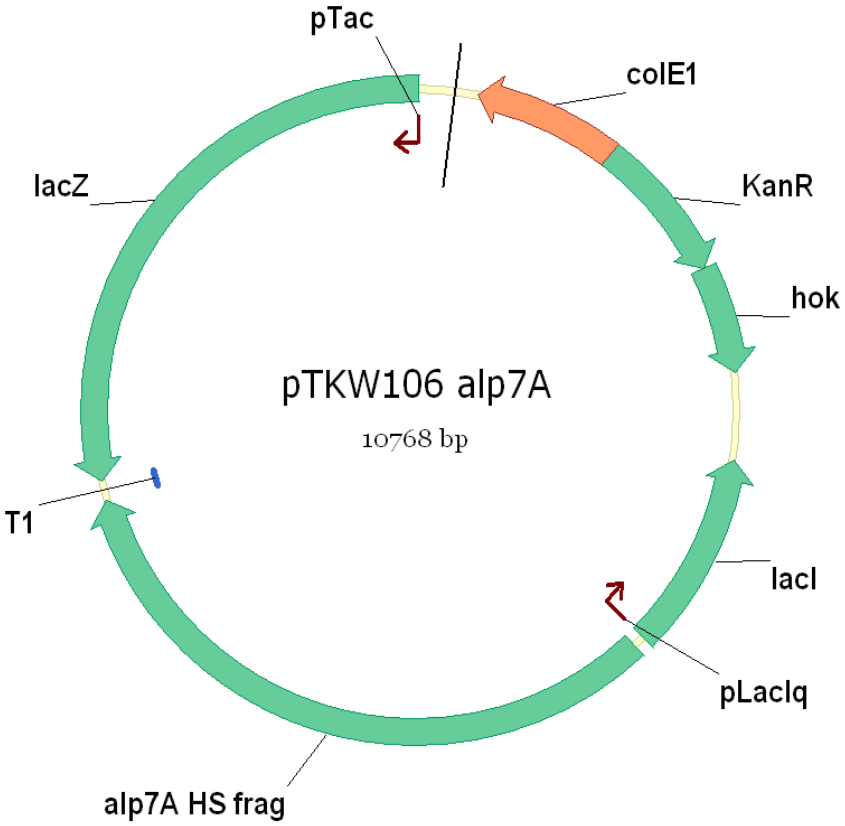

Fig. S1: Map of plasmid pTKW106 alp7A.

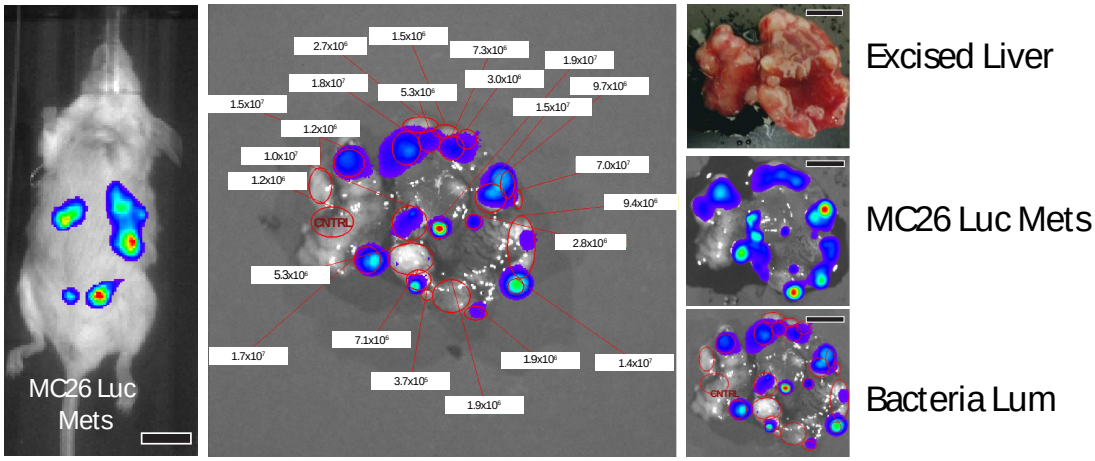

Fig. S2: Size and colonization of liver metastases. Mice with liver metastases (21 days) were injected intraperitonealy with luciferin and imaged using IVIS (left). Even in an intact host mouse, some liver metastases are visible. These signals derive from large tumors near the surface of the organ. 48 hours later, we orally administered PROP-Luc at $5x10^9$ CFU and waited an additional 24 hours for colonization to occur. To assay for correlation between tumor- and bacterial-derived luminescence, the liver was explanted and imaged using IVIS to first capture bacterial luminescence (Bacteria Lum image, bottom). The bacteria luxCDABE cassette produces luminescence without the addition of a substrate. We then soaked the liver in a D-luciferin solution after which luminescence derived from the firefly luciferase gene expressed by MC26-LucF cells was observed (MC26 Luc Mets, middle). Quantification of colonized metastases (middle, radiance values in p/sec/cm2/sr shown) is described in the Materials and Methods section and data is included in Table S1.

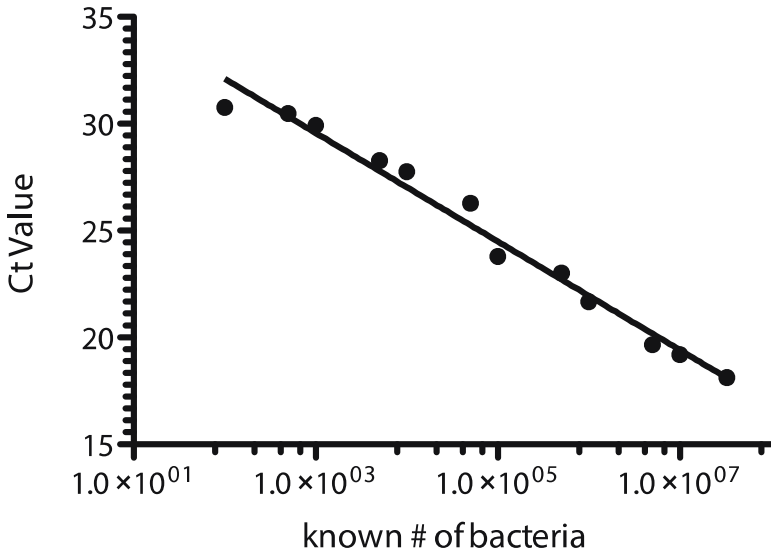

Fig. S3: Calibration curve for the qPCR calculation of the number bacteria in a tumor sample. Mean ± SEM, N=5 q-PCR replicates, error bars are smaller than the size of points.

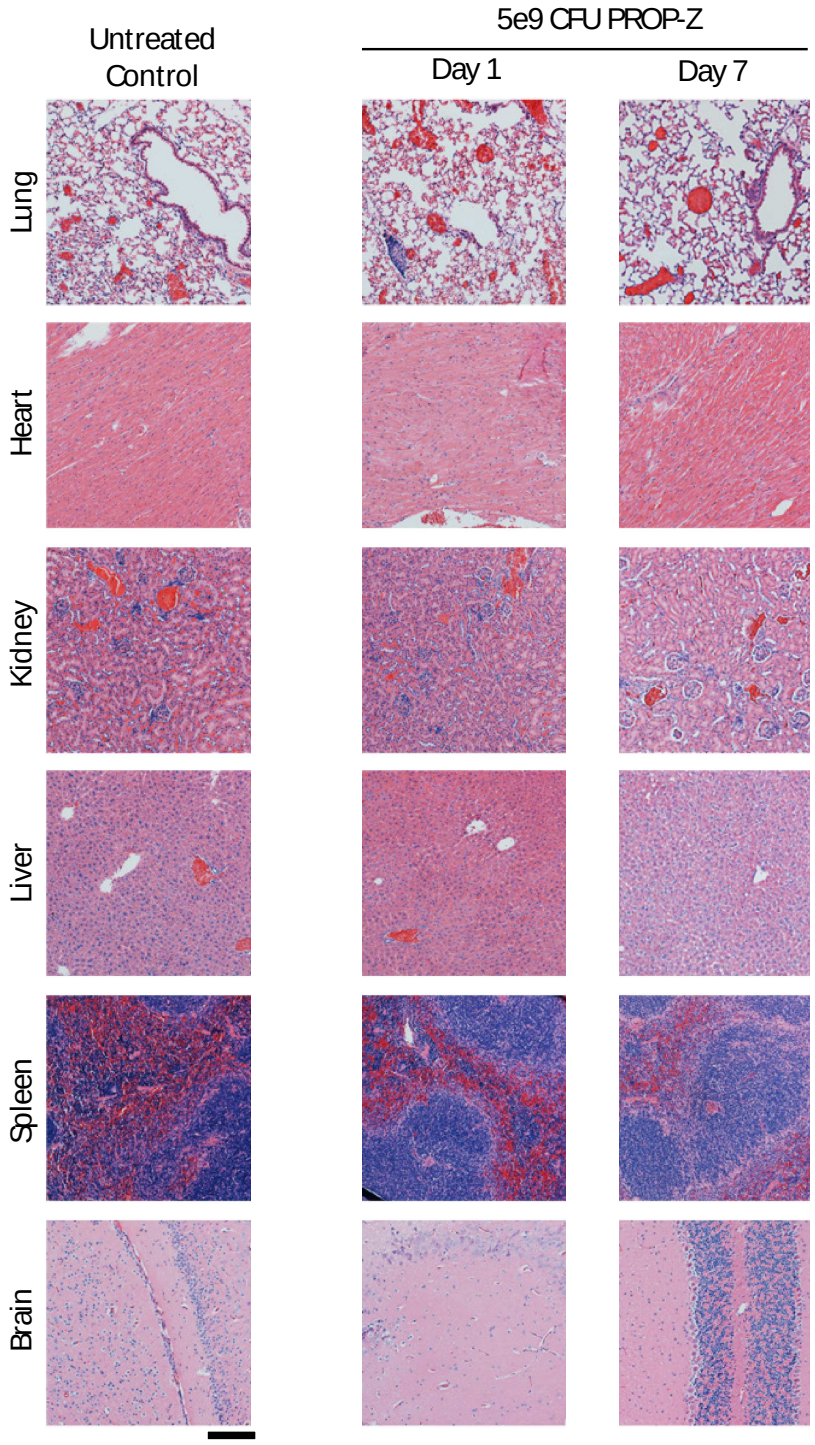

Fig. S4: Histopathological analysis of organs following oral delivery of PROP-Z. H&E staining of lungs, hearts, kidneys, livers, spleens, and brains of mice 1 and 7 days after oral gavage with $5x10^9$ PROP-Z, relative to untreated controls. Scale bar: 100 µm.

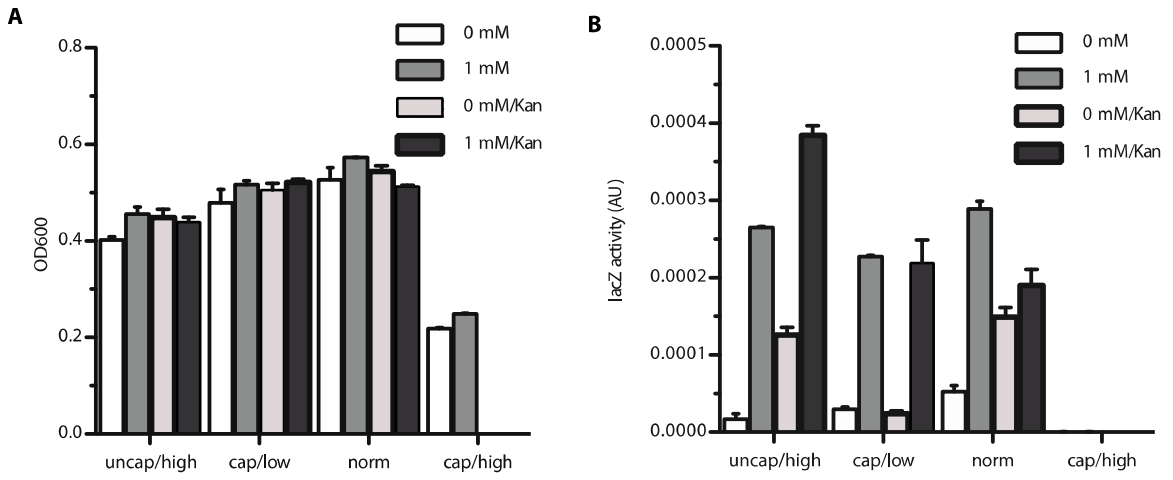

Fig. S5: Growth and activity of stabilized lacZ plasmid in different oxygen, inducer (IPTG), and antibiotic conditions. Oxygen conditions were varied for 48 hours by growing Mach1 (lacZ deficient) strain bacteria transformed with pTKW106alp7A in 14 mL Falcon tubes. These cultures were subcultured every 24 hours, and grown in tubes that were either capped or uncapped, and with either a high volume of media (14 mL) or low media volume (3 mL). Inducer (IPTG, 1.0 mM) and antibiotic (kanamycin, 50 ug/mL) conditions were also varied as indicated. Normal (norm) conditions are 3 mL media in an uncapped tube. Cultures were assayed for density (OD_{600}) in **(A)** and lacZ activity **(B)**. Mean ± SEM, N=3 for each column shown above.

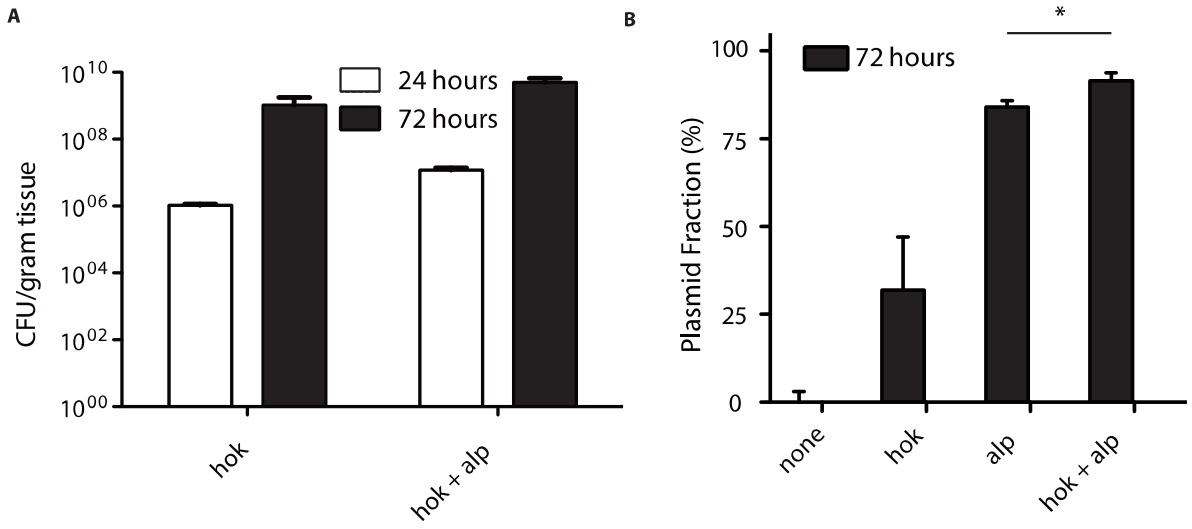

Fig. S6: CFU and stability of constructs in subcutaneous tumor models. Nude mice bearing subcutaneous tumors derived from the LS174T_LucF cell line were injected intravenously with $1x10^6$ PROP (EcN-luxCDABE) bacteria with either the pTKW106 (hok only), pTKW106alp7A (hok+alp), pTKW106_delhok (none), or pTK106alp7A (alone) plasmids. **(A)** Absolute levels of bacteria present in explanted, dissociated tumors were determined at two time points by colony counts in the presence of kanamycin and erythromycin. Growth rates of the bacteria bearing both stability plasmids are not slower than the parent strain. **B)** Plasmid stability was determined at 72 hours by performing differential colony counts in the presence of erythromycin (resistance gene present on integrated luxCDABE) or erythromycin and kanamycin (resistant only with the retention of pTKW106 plasmids). N=4-6 tumors in each column shown above, * indicates $P<0.05$, Student's t-test.

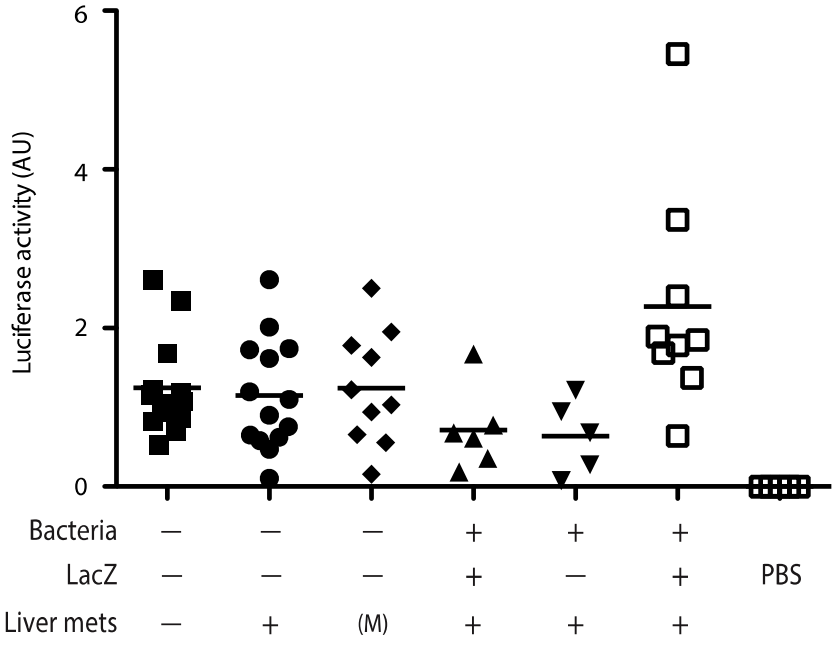

Fig. S7: Background cleavage of Lugal from urine assay. We performed assays on a variety of test cases to determine the dominant source of background cleavage of Lugal. The case without administration of PROP-Z to Liver Mets (-Bacteria, -lacZ, -LM), representing healthy mice, has the narrowest spread, and the introduction of the surgery procedure itself, either with cells (-Bacteria, -lacZ, +LM) or PBS (-Bacteria, -lacZ, Mock), generates variability into the urine cleavage assay. The PBS control shows an *in vitro* incubation of LuGal for 2 hours at room temperature with no significant LuGal cleavage observed. In vitro, we observed reporter cleavage by homogenized liver tissue from healthy mice, but no significant signals were obtained after incubation with whole blood. 3 way ANOVA was performed as in Table S2 where +PROPZ (+Bacteria, +LacZ) causes the most significant difference between +Liver Mets and – Liver Mets groups, $P < 0.005$.

	Df	Sum Sq	Mean Sq	F value	Pr(>F)
PROP-Z	1	2.975e+12	2.975e+12	4.324	0.04373
LM	1	1.304e+12	1.304e+12	1.896	0.17587
nonlacZ	1	2.394e+12	2.394e+12	3.480	0.06912
PROP-Z:LM	1	6.414e+12	6.414e+12	9.322	0.00392
Residuals	42	2.890e+13	6.881e+11		

Table S2. Results of three-way factorial ANOVA. We performed a 3 way ANOVA on PROP-Z, Liver Metastasis (LM), and nonlacZ variables from the data in Fig. S7. The P value (P=0.17587) indicates that the difference in urine assay value between liver metastasis and healthy mice before administration of PROP-Z is not statistically significant. Thus, the background cleavage of our substrate is mostly from a healthy mouse (-Bacteria, -lacZ, -Liver Metastasis). The introduction of PROP-Z causes the most significant difference between +LM and –LM experiment design (P=0.00392). Df=Degrees of Freedom, Sum Sq=Sum of the squares, Mean Sq=Mean of Sq, F-value=F-statistic, Pr (>F)=P-value.